Phase instabilities in semiconductor lasers: A codimension-2 analysis

L. Gil* and G. L. Lippi
Institut Non Linéaire de Nice, Université de Nice-Sophia Antipolis and CNRS, UMR 7735, 1361 Route des Lucioles, F-06560 Valbonne, France
(Received 26 September 2014; published 20 November 2014)

We compute the normal form description of a semiconductor laser near its threshold, with the sole assumption that the polarization be related to the electric field through the susceptibility (dependent on laser frequency and population inversion). We prove both analytically and numerically the possible existence of a phase-unstable regime, characterized by a periodic oscillation of the optical frequency and a constant intensity. This regime bears close resemblance to the mode-switching behavior, with constant total output power, experimentally observed in semiconductor lasers. In addition, our model predicts the appearance of a phase- and amplitude-turbulent regime, compatible with experimental observations. Both regimes are well known in fluid dynamics under the name Benjamin-Feir instability.

DOI: 10.1103/PhysRevA.90.053838 PACS number(s): 42.55.Px, 42.55.Ah, 42.60.Mi

I. INTRODUCTION

The *ideal* laser, unidirectional and operating on a single longitudinal and transverse mode, unperturbed by external noise, is reputed to operate in a stable continuous wave emission regime at least in a neighborhood of its threshold. This idealized picture originates on the one hand from the physics of class A lasers [1] and from experimental realizations where such a mode of operation is possible, and on the other hand, from the theoretical support lent by the paradigmatic, but ubiquitous, Maxwell-Bloch model based on the wave propagation equation and two levels interacting with the radiation field [2,3].

Real devices, however, behave in a way which is typically far from this idealized picture and semiconductor lasers never fulfill the framework of the *perfect* laser, unless serious technical efforts are put into stabilizing their temporal and spectral properties. Indeed, semiconductor lasers show, even at threshold, a dynamics which is typically multimode and quite complex. At first, the origin of this complexity was mainly attributed to external noise sources. During the 1980s and 1990s intensive work classified various kinds of semiconductor laser dynamics into two main categories: mode partition, where the total laser power fluctuates among several coexisting longitudinal modes [4,5], and mode hopping where only one mode at a time is emitting [5,6]. Optical reinjection, whether experimentally added or due to spurious backreflections, was recognized as being responsible for an extremely complex multimode dynamics [7], whose different regimes have been clarified by detailed investigations (cf. [8] for a summary): low-frequency fluctuations [9], mode hopping [10], coherent collapse [11], and fast phase jumps [12] with antiphase oscillations during the fast transient which wash out the details of the dynamics [13].

This picture appeared to offer a complete description of the physics and dynamics of multimode semiconductor lasers until, in 2004, experimental measurements conducted in *short wavelength* ($\lambda = 830$ nm) multiple quantum well (MQW) devices showed the presence of a deterministic dynamics in the modal switching [14,15]: The spectrally resolved measurements showed a periodic alternation from one mode to the subsequent one with almost no modulation in the total emitted output power (but nearly full modulation in the modal, i.e., frequency-resolved emission) with a sequence starting from the bluest to the reddest mode. As a function of the experimental parameters the regular frequency (phase) dynamics progressively develops an amplitude modulation, which eventually terminates in irregular behavior. An essentially similar mode of operation was reported also for *long wavelength* ($\lambda = 1.3\ \mu$m) MQW lasers [16], although the details are somewhat less clear in this paper. It is important to notice that this dynamics is not limited to MQW lasers, but that similar modal alternations, with nearly constant laser output, have also been reported in multimode quantum dot lasers [17].

In the absence of general modeling approaches, *ad hoc* models were developed to explain this dynamics on the basis of mode coupling induced either by four-wave mixing (FWM) [14] or by other nonlinear effects such as cross saturation (CS) and self-saturation (SS) [18]. This way, the individual modes are coupled through the material gain in a way which is obtained through a tailored description of the semiconductor nonlinear response using either phenomenological functional representations of its behavior, or expansions of the interaction terms expressed through the electric susceptibility, often expressed in approximate closed mathematical forms [19].

The second choice has gained in popularity, given its more rigorous treatment of the material properties, and forms now the basis on which other descriptions of modal dynamics rest. Common to all these approaches is the implicit assumption that the global field should be projected onto the ensemble of cavity modes and that the laser's response is properly characterized by the sum of the individual modal intensities. This assumption meets a restriction which has been common in experimental systems, where, up until very recently, the intermode beating was outside the reach of direct electrical measurements (and is still today difficult to achieve). Indeed, the intermode spacing is such that the high-frequency oscillations which would result from the interference between modes are averaged out in the detection process (both at the level of most transducers, as well as by the electrical bandwidth of the sampling and storing equipment).

*lionel.gil@inln.cnrs.fr

A new theoretical framework was proposed in 2006, bringing into play two complex Ginzburg-Landau equations (CGLEs) for the slowly varying amplitudes of the counterpropagating optical fields, coupled to an equation for the carrier population dynamics [20]. The use of the full electric field, rather than its projection onto the modal components, offers the advantage of intrinsically preserving the phase information without any approximations and of automatically including all those nonlinear effects which are approximately described by nonlinear expansions, such as FWM, CS, SS, etc. The model *appears* to correctly reproduce the anticorrelated oscillations of the modal intensities as well as the stationarity of the incoherent sum (i.e., the sum of the modal intensities as opposed to the intensity of the sum of the modes). However, this model does not include the possible destabilization of the monochromatic solution near threshold. Indeed, we have integrated the model equations [21] in the same parameter regimes shown in the paper [20] and have thereby proven that the previous observations simply correspond to a (long) transient: If the numerical integration runs for a sufficiently long time (cf. Appendix A), the phase dynamics relaxes toward a homogeneous, stationary steady state. Upon closer inspection of the model [20], one remarks that second-order spatial derivatives are kept for the diffusion contribution, while those for dispersion are neglected. Certainly, the dissipative contribution is essential to prevent small scale instabilities and neglecting them leads to the spontaneous generation of strong gradients and to quick numerical instabilities. However, this does not imply that conservative contributions are negligible, as we will prove later in the paper.

Building on this approach [20], but aware of the recent proof [22] that a conceptually crucial physical mechanism may entirely disappear when performing a cursory approximation which retains only the resonant terms, we apply a standard multiscale approach [23,24] directly onto the original set of equations describing the semiconductor dynamics and not, as in [20], onto the already reduced model. In our strategy, the total response of the medium is expressed as a function of the carrier density (in the usual way) and of the formal dependence of the medium's polarization on the total electric field (rather than on the modal superposition of its components) through the electric susceptibility. Since this dependence is treated formally, one can later choose to use an expression based on a mathematically approximated functional form [19], or on an experimentally measured response.

A detailed physical discussion can be found in [25]. Here, we concentrate on the mathematical derivation of the model, a technical and lengthy task, which requires a clear identification of all small quantities, and a good control of their respective smallness. At first sight, our final equations are quite similar to those of [20] and contain more or less the same terms, save for small, but crucial differences. A closer look at the equations' structure shows the existence of a new coefficient (which we name β) capable of driving the CGLE into a phase-unstable regime [26] (the phase instability is, for dissipative systems, the equivalent of self-focusing in conservative systems). This apparently minor change—resting on the complex nature of an otherwise real parameter in [20]—entirely changes the dynamics predicted by the model of the semiconductor laser. Indeed the phase portrait of the CGLE has been carefully explored over the years [27,28]: In the phase-stable regime, nontrivial phase dynamics can be observed only in the presence of large enough amplitude modulation. On the contrary, in the pure phase instability regime the monochromatic solution spontaneously destabilizes even near the laser threshold. As observed experimentally, this gives rise to a periodic, asymmetric oscillation of the electric field's frequency, while its intensity (and not the sum of the modal intensities) remains nearly constant.

The semiconductor laser dynamics have both random and deterministic features. Random aspects were first identified and modeled [4–6,29–31] and naturally, when discovered [14–17], the deterministic aspects were mainly interpreted as being of different nature (except in [32]). Our treatment does not make use of any external noise sources, but the phase instability dynamics, which emerges from the coherent derivation of the full equations, has long ago been recognized to be a strong source of intrinsic noise [33]. Without refuting the existence of genuine extrinsic noise sources [34,35], our approach reconciles, in some way, the two apparently contradicting aspects of the problem, since it shows that an apparently random behavior can emerge from the deterministic component. It also poses new questions on the relative importance of the deterministic and material-related noise sources.

The paper is organized as follows. In Sec. II we present the derivation of the reduced dynamics near the laser threshold [36]. In particular, we focus on the choice of scaling laws (Sec. II C), on the derivation of the polarization expression from the electric susceptibility, and on the organizational structure of the whole calculation. Technical details are reported in Appendices B and C. We then extract some analytical solutions to the reduced equations and investigate the linear stability of the basic continuous wave solution (Sec. III A), showing the generic possibility (Sec. III B) for the existence of a phase instability regime [26]. Developing in Sec. III C the analogy with the CGLE (subject of numerous investigations), we predict the existence of two unstable phase regimes which differ by the dynamics of the intensity, either constant or turbulent, and we propose that the "intrinsic noise" generated by the phase instability may play the role usually attributed in semiconductor laser dynamics to the physical noise sources. Finally, before concluding (Sec. IV) we present in Sec. III D numerical simulations of our model in the various predicted parameter regimes and discuss them in relationship with the experimental observations.

II. NORMAL FORM DESCRIPTION

A. Basic equations

The wave equation for an electric field E polarized along the x axis and propagating along the z direction takes the form

$$\partial_{tt} E + \frac{1}{\epsilon_0} \partial_{tt} P = c^2 \partial_{zz} E - \sigma \partial_t E, \tag{1}$$

where P is the medium's polarization density, σ represents Ohmic losses (and all other additional sources of energy dissipation), ϵ_0 is the vacuum's permittivity, and c is the speed of light (in vacuum).

The evolution equation for the population inversion N reads

$$\partial_t N = \gamma(N_p - N) + D\partial_{zz}N + \frac{2}{\hbar\omega_c} E\partial_t P, \tag{2}$$

where ω_c is the electric field's operating frequency, N_p represents the pump rate, D is the material's diffusion constant for the carriers, and $\hbar$ is the reduced Planck constant. Although analytical calculations [37] and experimental observations (e.g., [38]) give direct access to the susceptibility, many semiconductor models (e.g., [39]) begin by proposing an approximate dynamics for the polarization variable. Here, following [40], we directly manipulate the polarization through

$$\widehat{P}(\omega) = \epsilon_0 \chi(\omega, N)\widehat{E}(\omega). \tag{3}$$

B. At threshold

The simplest, basic solution to Eqs. (1) and (2) is given by $N = N_p$ and $E = P = 0$. Looking for a nontrivial solution of the form

$$E = \mathcal{E}e^{i(\omega t - kz)}, \quad P = \epsilon_0 \mathcal{E}\chi(\omega, N_p)e^{i(\omega t - kz)} \tag{4}$$

we obtain the following solvability condition which ensures the existence of a nonvanishing solution:

$$\big[-\omega^2 - \chi(\omega, N_p)\omega^2 + c^2k^2 + i\sigma\omega\big]\mathcal{E} = 0. \tag{5}$$

We define N_{pc} as the smallest value of N_p for which the equation

$$\chi_i(\omega, N_{pc}) = \frac{\sigma}{\omega} \tag{6}$$

possesses a solution in ω (χ_i stands for the imaginary part of χ). The values of ω satisfying this condition are defined as $\pm\omega_c$. By construction, when this condition is satisfied

$$\left.\frac{\partial \chi_i}{\partial \omega}\right|_{\pm\omega_c, N_{pc}} = 0 \tag{7}$$

and

$$\frac{\omega_c^2}{c^2}[1 + \chi_r(\omega_c, N_{pc})] = k_c^2 \tag{8}$$

defines the critical eigenvector k_c, where χ_r stands for the real part of χ.

C. Scalings

Close to the laser bifurcation, there are three independent slow characteristic times:

(1) A first one associated with the electric field amplitude's growth rate and related to the distance ($dN = N_p - N_{pc}$) to the laser threshold.

(2) A second one related to the population inversion (γ^{-1}).

(3) A third characteristic time which does not appear explicitly. In fact, this characteristic time scale is associated with the shape of the susceptibility curves near the resonance frequency. Hence $\frac{\partial\chi}{\partial\omega}|_{\omega_c, N_{pc}} \propto \frac{1}{\Gamma}$ and $\frac{\partial^2\chi}{\partial\omega^2}|_{\omega_c, N_{pc}} \propto \frac{1}{\Gamma^2}$, where Γ is typically of the order of 10^{12} Hz for semiconductor lasers. Close enough to the laser threshold and assuming unidirectional emission, we expect the electric field amplitude to be expressed as

$$E = \mathcal{E}e^{i(\omega_c t - k_c z)} + \mathcal{E}^* e^{-i(\omega_c t + k_c z)} + \cdots, \tag{9}$$

where $\mathcal{E}$ is slowly varying with space and time. The restriction to slow spatiotemporal variations is equivalent to saying that the corresponding Fourier component $\widehat{\mathcal{E}}(\omega)$ is nonvanishing only in a small neighborhood of the origin. Following the approach developed in [41], we derive

$$\begin{aligned}
\frac{P(t)}{\epsilon_0} &= \int \chi(\omega)\widehat{E}(\omega)e^{i\omega t}d\omega \\
&= e^{+i(\omega_c t - k_c z)}\int \chi(\omega)\widehat{\mathcal{E}}(\omega - \omega_c)e^{i(\omega-\omega_c)t}d\omega + e^{-i(\omega_c t - k_c z)}\int \chi(\omega)\widehat{\mathcal{E}}^*(\omega + \omega_c)e^{i(\omega+\omega_c)t}d\omega \\
&= e^{+i(\omega_c t - k_c z)}\int \left[\chi(\omega_c, N) + \left.\frac{\partial\chi}{\partial\omega}\right|_{\omega_c, N}\frac{(\omega-\omega_c)}{1!} + \left.\frac{\partial^2\chi}{\partial\omega^2}\right|_{\omega_c, N}\frac{(\omega-\omega_c)^2}{2!} + \left.\frac{\partial^3\chi}{\partial\omega^3}\right|_{\omega_c, N}\frac{(\omega-\omega_c)^3}{3!} + \cdots\right] \\
&\quad \times \widehat{\mathcal{E}}(\omega - \omega_c)e^{i(\omega-\omega_c)t}d\omega + \text{c.c.} \\
&= e^{+i(\omega_c t - k_c z)}\left[\chi(\omega_c, N)\mathcal{E} + \frac{1}{1!}\left.\frac{\partial\chi}{\partial\omega}\right|_{\omega_c, N}\left(\frac{\partial_t}{i}\right)\mathcal{E} + \frac{1}{2!}\left.\frac{\partial^2\chi}{\partial\omega^2}\right|_{\omega_c, N}\left(\frac{\partial_t}{i}\right)^2\mathcal{E} + \frac{1}{3!}\left.\frac{\partial^3\chi}{\partial\omega^3}\right|_{\omega_c, N}\left(\frac{\partial_t}{i}\right)^3\mathcal{E} + \cdots\right] + \text{c.c.}
\end{aligned} \tag{10}$$

Looking for a solution of Eq. (1) under the form $E = e^{\lambda t}e^{ikz}$ where $N = N_{pc} + dN$, $\lambda = i\omega_c + d\lambda$, and $k = k_c + dk$, and taking full advantage of Eq. (10) we obtain

$$\frac{d\lambda}{\omega_c}\left[2i(1+\chi) + i\omega_c\frac{\partial\chi}{\partial\omega} + \frac{\sigma}{\omega_c}\right] = N_{pc}\frac{\partial\chi}{\partial N}\frac{dN}{N_{pc}} - 2\frac{c^2k_c^2}{\omega_c^2}\frac{dk}{k_c}, \tag{11}$$

where we have used the following notation convention: when χ or any of its derivatives are evaluated at ω_c, N_{pc} we write χ, $\frac{\partial\chi}{\partial N}\ldots$ instead of $\chi(\omega_c, N_{pc})$, $\frac{\partial\chi}{\partial N}|_{\omega_c, N_{pc}}\ldots$. Then taking into account the smallness of the experimentally fixed parameters

$$\frac{\gamma}{\omega_c} \simeq 10^{-6}, \quad \simeq 10^{-3}, \quad \simeq 10^{-3}, \quad \simeq 10^{-3} \tag{12}$$

[note that $(\frac{\gamma}{\omega_c})^{1/2} \simeq (\frac{\Gamma}{\omega_c}) \simeq (\frac{\sigma}{\omega_c})$] we obtain

$$\frac{d\lambda}{\omega_c} \propto \left(\frac{\Gamma}{\omega_c}\right)\frac{dN}{N_{pc}}, \quad \frac{dk}{k_c} \propto \frac{dN}{N_{pc}}, \tag{13}$$

which implies that the nth term in the power expansion, Eq. (10) is proportional to

$$\left(\omega_c\frac{\partial\chi}{\partial\omega}\right)^n\left(\frac{\partial_t-i\omega_c}{i\omega_c}\right)^n\propto\left(\frac{\omega_c}{\Gamma}\right)^n\left(\frac{d\lambda}{\omega_c}\right)^n\propto\left(\frac{dN}{N_{pc}}\right)^n \quad (14)$$

and is, *a posteriori*, consistent with its convergence. From the equilibrium condition for the carrier density, Eq. (2),

$$\gamma(N-N_p)\propto\frac{2}{\hbar\omega_c}E\partial_t P\Longrightarrow\gamma N_{pc}\,\frac{dN}{N_{pc}}\propto\frac{\epsilon_0}{\hbar}\chi_i E^2 \quad (15)$$

we can estimate the leading amplitude term in the expansion for the electric field

$$E\propto\sqrt{\frac{\omega_c\hbar N_{pc}}{\epsilon_0}}\left(\frac{\gamma}{\sigma}\right)^{1/2}\left(\frac{dN}{N_{pc}}\right)^{1/2}. \quad (16)$$

Hence, the amplitude and the time and space evolution of the electric field possess a functional dependence on $\frac{dN}{N_{pc}}$.

The usual mathematical procedures to reduce the dynamics to its essentials are based on a direct adiabatic elimination of the fast variables and those situations where the characteristic times are well separated have therefore been intensively studied [42]. Here, we adopt a diametrically opposite, but nevertheless well established [23,24], viewpoint: When approaching the laser threshold we seek to slow down the electric field's envelope dynamics (controlled by $\frac{dN}{N_{pc}}$) until it becomes as slow as the population inversion's (controlled by $\frac{\gamma}{\omega_c}$). Note that this choice is ideal for numerical simulations, since the resulting unique characteristic time allows for the use of efficient algorithms. This choice is also interesting from an analytical point of view because it does not drastically shrink the phase space, but, rather, fully analyzes it on a unique time scale.

Even if the two characteristic times have to be small at the same time, they are not forced to vanish with the same velocity. As usual in codimension-2 analysis, there is not a rigorous, fully satisfactory way of selecting the ratio r between the two characteristic time scales

$$\frac{dN}{N_{pc}}=\left(\frac{\gamma}{\omega_c}\right)^r. \quad (17)$$

Several values of r are possible and each choice leads to a slightly different end result. Globally, the final normal form equations always contain the same terms, but each term's rank in the power expansion may change depending on the choice of r.

We have investigated three distinct values of r: $\frac{3}{2}$, $\frac{1}{2}$, and $\frac{1}{3}$. Here, we explicitly discuss the case $r=\frac{1}{2}$, which turns out to be a good compromise between physical accuracy and computational difficulty. The other two remaining values are considered in Appendices B and C.

The following scalings are now introduced:

$$\begin{aligned}
&\gamma=\omega_c\epsilon^2 \quad \text{definition of } \epsilon,\\
&N_p=N_{pc}(1+\widetilde{\mu}\epsilon) \quad \text{with } \widetilde{\mu}\simeq O(1),\\
&\sigma=\omega_c\epsilon\widetilde{\sigma}\Longrightarrow\chi_i=\frac{\sigma}{\omega_c}=\epsilon\widetilde{\sigma},\\
&\Gamma=\omega_c\epsilon\widetilde{\Gamma},\\
&D=\epsilon\frac{\omega_c}{k_c^2}\widetilde{D}
\end{aligned} \quad (18)$$

with

$$\begin{aligned}
N&=N_{pc}(1+\epsilon^1S+\epsilon^2N_2+\cdots),\\
E&=\sqrt{\frac{\omega_cN_{pc}\hbar}{\epsilon_0}}(\epsilon^1E_1+\epsilon^2E_2+\cdots),\\
P&=\epsilon_0\sqrt{\frac{\omega_cN_{pc}\hbar}{\epsilon_0}}(\epsilon^1P_1+\epsilon^2P_2+\cdots),
\end{aligned} \quad (19)$$

and

$$\begin{aligned}
\partial_t&=\omega_c\Big(\partial_{t_0}+\underbrace{\epsilon^2\partial_{t_2}+\epsilon^3\partial_{t_3}+\epsilon^4\partial_{t_4}+\cdots}_{\epsilon^2\partial_T}\Big),\\
\partial_z&=k_c\Big(\partial_{z_0}+\underbrace{\epsilon^1\partial_{z_1}+\epsilon^2\partial_{z_2}+\epsilon^3\partial_{z_3}+\cdots}_{\epsilon\partial_Z}\Big).
\end{aligned} \quad (20)$$

Further, we introduce the dimensionless partial derivatives

$$\omega_c\frac{\partial\chi}{\partial\omega}\bigg|_{\omega_c,N}=\frac{\chi_\omega(N)}{\epsilon},\quad \omega_c^2\frac{\partial^2\chi}{\partial\omega^2}\bigg|_{\omega_c,N}=\frac{\chi_{\omega\omega}(N)}{\epsilon^2}, \quad (21)$$

so that $\chi_\omega(N)$ and $\chi_{\omega\omega}(N)$ are now of order 1.

In rescaled units, Eq. (10) now takes the form

$$P=e^{+i(t_0-z_0)}\begin{bmatrix}\chi(\omega_c,N)\\ +\frac{1}{1!}\chi_\omega(N)(-i\epsilon\partial_T)\\ +\frac{1}{2!}\chi_{\omega\omega}(N)(-i\epsilon\partial_T)^2\\ +\frac{1}{3!}\chi_{\omega\omega\omega}(N)(-i\epsilon\partial_T)^3\\ +\cdots\end{bmatrix}\mathcal{E}+\text{c.c.} \quad (22)$$

Taking into account all the previous scalings, Eqs. (1) and (2) become

$$\begin{aligned}
&\big[\partial_{t_0t_0}+2\epsilon^2\partial_{t_0t_2}+2\epsilon^32\partial_{t_0t_3}+\epsilon^4\big(2\partial_{t_0t_4}+\partial_{t_2t_2}\big)\cdots\big][\epsilon^1(E_1+P_1)+\epsilon^2(E_2+P_2)+\cdots]\\
&\quad=-\epsilon\widetilde{\sigma}\big[\partial_{t_0}+\epsilon^2\partial_{t_2}+\epsilon^3\partial_{t_3}+\cdots\big][\epsilon E_1+\epsilon^2E_2+\cdots]+\frac{c^2k_c^2}{\omega_c^2}\big[\partial_{z_0z_0}+2\epsilon^1\partial_{z_0z_1}+\epsilon^2\big(2\partial_{z_0z_2}+\partial_{z_1z_1}\big)+\cdots\big][\epsilon^1E_1+\epsilon^2E_2+\cdots],\\
&\big[\partial_{t_0}+\epsilon^2\partial_{t_2}+\epsilon^3\partial_{t_3}+\cdots\big][\epsilon^1S+\epsilon^2N_2+\epsilon^3N_3+\cdots]\\
&\quad=\epsilon^2[\epsilon(\widetilde{\mu}-S)-\epsilon^2N_2-\epsilon^3N_3\cdots]+\epsilon\widetilde{D}\big[\partial_{z_0z_0}+2\epsilon^1\partial_{z_0z_1}+\epsilon^2\big(2\partial_{z_0z_2}+\partial_{z_1z_1}\big)+\cdots\big][\epsilon S+\epsilon^2N_2+\epsilon^3N_3+\cdots]\\
&\qquad+2[\epsilon E_1+\epsilon^2E_2+\cdots]\big[\partial_{t_0}+\epsilon^2\partial_{t_2}+\epsilon^3\partial_{t_3}+\cdots\big][\epsilon P_1+\epsilon^2P_2+\epsilon^3P_3+\cdots].
\end{aligned} \quad (23)$$

D. Resolution of the hierarchy of equations

The previous system of equations (23), together with the expansion (22), has to be solved order by order. We thus obtain a hierarchy of linear partial differential equations which can be successively solved, provided that suitable solvability conditions are satisfied. It is worth noting that the aim of the computation is not to find all the solutions, but, on the contrary, to find under which conditions a given expansion—which is to be chosen in the most convenient way—is solution.

At order ϵ^1 we obtain

$$\partial_{t_0 t_0}(E_1+P_1)=\frac{c^2k_c^2}{\omega_c^2}\partial_{z_0 z_0}E_1,$$
$$\partial_{t_0}S=0. \tag{24}$$

Choosing

$$E_1=F(sv)e^{+i(t_0-z_0)}+\text{c.c.}, \tag{25}$$

where $sv=t2,t3,t4\cdots z1,z2,z3,\ldots$ stands for all the slow variables, and substituting into (22) leads to

$$P_1=\chi_r F e^{+i(t_0-z_0)}+\text{c.c.} \tag{26}$$

Then the solvability condition for Eqs. (24) is

$$1+\chi_r(\pm\omega_c,N_{pc})=\frac{c^2k_c^2}{\omega_c^2}, \tag{27}$$

which is obviously satisfied because of Eq. (8) and

$$\partial_{t_0}S=0. \tag{28}$$

At order ϵ^2 we get

$$\partial_{t_0 t_0}(E_2+P_2)=-\widetilde{\sigma}\partial_{t_0}E_1+\frac{c^2k_c^2}{\omega_c^2}\left(\partial_{z_0 z_0}E_2+2\partial_{z_0 z_1}E_1\right),$$
$$\partial_{t_0}N_2=\widetilde{D}\partial_{z_0 z_0}S+2E_1\partial_{t_0}P_1. \tag{29}$$

Searching for E_2 of the form

$$E_2=F_2(sv)e^{i(t_0-z_0)}+\text{c.c.} \tag{30}$$

leads to

$$P_2=\left[\chi_r F_2+i\widetilde{\sigma}F+\frac{\partial\chi}{\partial N}N_{pc}SF-i\chi_\omega\partial_{t_2}F\right]e^{i(t_0-z_0)}+\text{c.c.} \tag{31}$$

The solvability conditions are expressed by

$$\partial_{t_2}F=-V\partial_{z_1}F+c_0SF,$$
$$\partial_{z_0}S=0 \tag{32}$$

with

$$c_0=\frac{-i\frac{\partial\chi}{\partial N}N_{pc}}{\chi_\omega},\quad V=\frac{2c^2k_c^2}{\omega_c^2\chi_\omega}. \tag{33}$$

Under these conditions, a possible solution is

$$F_2=0,\quad N_2=\chi_r F^2 e^{2i(t_0-z_0)}+\text{c.c.} \tag{34}$$

and

$$P_2=e^{i(t_0-z_0)}\left[i\widetilde{\sigma}F+\frac{2ic^2k_c^2}{\omega_c^2}\partial_{z_1}F\right]+\text{c.c.} \tag{35}$$

At order ϵ^3 we have

$$\partial_{t_0 t_0}(E_3+P_3)+2\partial_{t_0 t_2}(E_1+P_1)$$
$$=+\frac{c^2k_c^2}{\omega_c^2}\left[\partial_{z_0 z_0}E_3+\left(2\partial_{z_0 z_2}+\partial_{z_1 z_1}\right)E_1\right],$$
$$\partial_{t_0}N_3+\partial_{t_2}S=\widetilde{\mu}-S+\widetilde{D}\partial_{z_0 z_0}N_2+2E_1\partial_{t_0}P_2. \tag{36}$$

Assuming $E_3=F_3e^{i(t_0-z_0)}+F_{33}e^{3i(t_0-z_0)}+\text{c.c.}$, we are left with

$$P_3=e^{i(t_0-z_0)}\begin{bmatrix}\chi_r F_3+N_{pc}\frac{\partial\chi}{\partial N}[N_2E_1]_1+\frac{N_{pc}^2}{2}\frac{\partial^2\chi}{\partial N^2}S^2F\\ -i\chi_\omega\partial_{t_3}F-iN_{pc}\frac{\partial\chi_\omega}{\partial N}S\partial_{t_2}F\\ -\frac{1}{2}\chi_{\omega\omega}\partial_{t_2 t_2}F\end{bmatrix}$$
$$+e^{3i(t_0-z_0)}\left[\chi(3\omega_c,N_{pc})F_{33}+\frac{\partial\chi}{\partial N}[N_2E_1]_3\right]+\text{c.c.} \tag{37}$$

The new terms of the form $[N_2E_1]_n$ represent in compact form the contributions of order n ($e^{ni(t_0-z_0)}$) coming from the product of N_2 [Eq. (34)] and E_1 [Eq. (25)].

$$[N_2E_1]_1=\chi_r|F|^2F. \tag{38}$$

Then the solvability conditions take the form

$$i\chi_\omega\partial_{t_3}F=N_{pc}\frac{\partial\chi}{\partial N}\chi_r|F|^2F+\frac{N_{pc}^2}{2}\frac{\partial^2\chi}{\partial N^2}S^2F$$
$$-iN_{pc}\frac{\partial\chi_\omega}{\partial N}S\partial_{t_2}F-\frac{1}{2}\chi_{\omega\omega}\partial_{t_2 t_2}F$$
$$-2i(1+\chi_r)\partial_{t_2}F+\frac{c^2k_c^2}{\omega_c^2}(-2i\partial_{z_2}F+\partial_{z_1 z_1}F),$$
$$\partial_{t_2}S=\widetilde{\mu}-S-4\widetilde{\sigma}|F|^2-\frac{4c^2k_c^2}{\omega_c^2}\partial_{z_1}|F|^2. \tag{39}$$

In the carrier density equation, the term proportional to $\partial_{z_1}|F|^2$ represents radiation pressure. This force does exist in an actual laser, but is normally compensated for by physical mechanisms (e.g., the crystal matrix when dealing with a solid-state laser) which are not taken into account in our initial description, Eq. (2). The equation for $\partial_{t_3}F$ contains a large number of terms, fortunately small compared to those of $\partial_{t_2}F$. Some represent additional saturation terms ($|F|^2F, S^2F$), others are just a straightforward renormalization of the group velocity ($\partial_{t_2}F$). Here, we only retain those physical terms which are not already present in Eq. (32): $\partial_{z_1 z_1}F$, which describes the dispersion and, possibly, diffusion of the electric field, and $iS\partial_{z_1}F$, which stands for the drift of the selected wavelength with S. Collecting all terms, we are left with

$$\partial_T F=-V\partial_Z F+c_0SF+i\epsilon c_{2i}S\partial_Z F+\epsilon c_1\partial_{ZZ}F,$$
$$\partial_T S=\widetilde{\mu}-S-4\widetilde{\sigma}|F|^2 \tag{40}$$

with

$$c_1=\frac{iV}{2}\left(\frac{\chi_{\omega\omega}V}{\chi_\omega}-1\right),\quad c_2=\frac{-i\chi_{\omega\omega}Vc_0}{\chi_\omega}+\frac{N_{pc}\frac{\partial\chi_\omega}{\partial N}V}{\chi_\omega}. \tag{41}$$

Note that for this particular scaling choice ($r=\frac{1}{2}$), and keeping terms up to $O(\epsilon^3)$, diffusion does not play a role

in the carrier density dynamics. No problem stemming from the lack of a diffusion term was detected in our numerical simulations. However, if needed, carrier density diffusion can be recovered, either by extending the analysis to higher orders in ϵ, or by selecting a different scaling choice (Appendix C).

III. DISCUSSION AND COMPARISON WITH EXPERIMENTS

A. Homogeneous solution and linear stability

The system describing the laser dynamics, Eqs. (40), possesses a one-parameter family of nonvanishing homogeneous solutions:

$$F = \sqrt{\frac{\widetilde{\mu}}{4\widetilde{\sigma}}}e^{i\phi}, \quad S = 0. \tag{42}$$

We now analyze the linear stability of the particular nonvanishing solution $\phi = 0$:

$$F = \left[\sqrt{\frac{\widetilde{\mu}}{4\widetilde{\sigma}}} + \eta(f_x + if_y)\right]e^{ikz}e^{\lambda(k)t},$$
$$S = \eta s e^{ikz}e^{\lambda(k)t}, \tag{43}$$

where k stands for the perturbation wave vector, η is the perturbation amplitude (assumed to be small), and $\lambda(k)$ represents the temporal evolution. We are especially interested in the critical eigenvalue (λ_ϕ) associated with the time translation invariance symmetry of Eq. (40) and characterized by $\lambda_\phi(k = 0) = 0$. Looking for λ_ϕ as an expansion in k, we obtain

$$\lambda_\phi = [l_2k^2 + l_4k^4 + O(k^6)] + i[-Vk + O(k^5)], \tag{44}$$

with

$$l_2 = -\epsilon\frac{c_{0r}c_{1r} + c_{0i}c_{1i}}{c_{0r}},$$
$$l_4 = -\epsilon^2\frac{c_{1i}^2\left(c_{0r}^2 + c_{0i}^2\right)}{2c_{0r}^3\widetilde{\mu}}. \tag{45}$$

Some important remarks are now in order:

(1) l_4 is always negative and corresponds to small space scale dissipation.

(2) l_2 gives the usual *Benjamin-Feir* phase instability criterion [26]. Negative values of l_2 correspond to the stability of the homogeneous nonvanishing solution, while positive ones are associated with a phase-unstable regime with possible oscillations in the optical frequency (as observed in [14–17]).

(3) The crucial difference between Eqs. (40) and those of [20] lies in the existence of c_{1i}, the imaginary part of c_1. Indeed, if $c_{1i} = 0$ the leading term in $\mathrm{Re}\{\lambda_\phi\} < 0$ and the monochromatic solution remains stable, as in [20], although long transients ($\lambda_\phi \propto \frac{\epsilon}{L^2}$, L laser length) may be mistaken for multimode dynamics (cf. Fig. 3, Appendix A, and Ref. [21]).

(4) $l_2 > 0$ if $\beta < -\frac{1}{\alpha} < 0$, thus the instability is controlled by the ratio $\frac{c_{1i}}{c_{1r}}$ rather than by the absolute value of $|c_1|$ (which may be very small).

(5) In the phase-unstable regime, the wave vector with the highest growth rate ($\max\{\mathrm{Re}(\lambda_\phi)\}$) is approximately given by

$$k_{\max}^2 \simeq -\frac{l_2}{2l_4}. \tag{46}$$

Substitution of this expression into $\mathrm{Im}(\lambda_\phi)$ leads to a periodic oscillation of the electric field with frequency

$$\Omega \simeq Vk_{\max}. \tag{47}$$

Notice that this frequency can become as small as desired as l_2 approaches zero. This feature closely matches the experimental observations, since the frequencies with which the lasing modes cycle [14,15] are at least three orders of magnitude smaller than the inherent oscillation frequencies typical of semiconductor lasers. As such, this observation was one of the most striking characteristics of the experimental findings [14,15] and one which was most difficult to interpret physically.

(6) The coefficient c_0 can be reexpressed as

$$c_0 = \frac{-iN_{pc}\frac{\partial\chi}{\partial N}}{\chi_\omega} = \frac{N_{pc}\frac{\partial\chi_i}{\partial N}}{\chi_\omega}(1 - i\alpha), \tag{48}$$

where α is almost [43] the usual alpha factor; $\frac{\partial\chi_i}{\partial N}$ is positive because, near the threshold, the gain increases with population inversion. χ_ω is real by construction and turns out to be positive (e.g., by computing it from the simple analytical expression of Ref. [19]).

(7) Examining c_1, we obtain

$$c_1 = \frac{iV}{2}\left(\frac{\chi_{\omega\omega}V}{\chi_\omega} - 1\right) = \frac{-V\chi_{i\omega\omega}}{2\chi_\omega}(1 - i\beta), \tag{49}$$

with

$$\beta = \frac{\chi_\omega}{V\chi_{i\omega\omega}}\left(\frac{\chi_{r\omega\omega}V}{\chi_\omega} - 1\right). \tag{50}$$

The real part of c_1 is associated with the curvature of the gain curve with respect to the frequency. As $\chi_{i\omega\omega} < 0$, the real part is positive, as expected. This means that as soon as the wave vector deviates from its critical value k_c (and therefore the frequency deviates from ω_c), the gain decreases as $-c_{1r}(k - k_c)^2$.

(8) l_2 can be reexpressed as

$$l_2 = -\epsilon c_{1r}(1 + \alpha\beta). \tag{51}$$

Therefore from the point of view of the spatiotemporal dynamics, the β coefficient is at least as important as the α coefficient, since it is the product $\alpha\beta$ which determines the stability of the solution. This new β parameter turns out to be an essential characteristic of semiconductor lasers. Evidence of its existence and its analytical expression is the main result of our analysis.

B. Does the phase instability regime exist?

In order to estimate realistic physical values for β, thereby assessing the possibilities for $l_2 > 0$, we consider the analytical approximation for the susceptibility in MQW lasers [19,44]:

$$\chi(\omega, N) = -\chi_0\left[2\ln\left(1 - \frac{v}{u - i}\right) - \ln\left(1 - \frac{B}{u - i}\right)\right], \tag{52}$$

where χ_0 is constant, $v = \frac{N}{N_t}$, $u = \frac{\omega - \frac{E_t}{\hbar}}{\Gamma}$, and B is a constant which depends on k_m the maximum wave vector contained in the first Brillouin zone, on the effective electron mass m_{eff} and

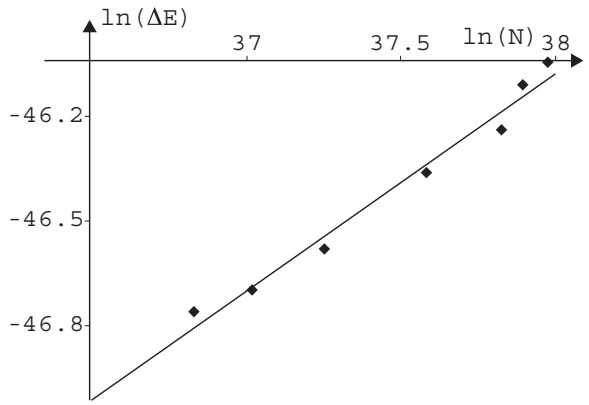

FIG. 1. Experimental data of the band-gap renormalization of a 103 Å $GaAs/Ga_{1-x}Al_xAs$ quantum well at 300 K extracted from [45] and replotted to provide the required information. The plot displays $\ln(\Delta E)$ versus $\ln(N)$, where $\Delta E = E_t(0) - E_t(N)$ is expressed in Joule and N, the surface charge density, in m^{-2} [Eq. (53)]. The continuous line is the linear best fit. The fitting parameters are $\ln(a) = -70 \pm 1$ and $b = 0.62 \pm 0.03$.

on Γ. Band-gap renormalization effects due to the screened Coulomb interaction between electrons and holes can be taken into account by renormalizing the transition energy E_t:

$$E_t(N) = \hbar\omega_t - aN^b \Longrightarrow u = \frac{\omega - \omega_t}{\Gamma} + p_s\left(\frac{N}{N_t}\right)^b, \quad (53)$$

where $p_s = (\frac{aN_t^b}{\hbar\Gamma})$ is the band-gap shrinkage parameter [19]. The coefficients a and b are material dependent and can be experimentally determined from [45,46] (Figs. 1 and 2). For the other parameters entering the evaluation of the stability properties (52), we use $N_t = 0.5\ 10^{15}\ m^{-2}$ (surface carrier density at transparency), $\omega_t = 0.63 \times 10^{15}$ Hz, $m_{\text{eff}} = m_e$, $k_m = 0.58 \times 10^{10}\ m^{-1}$, and $\chi_0 = 1$. With this set of data,

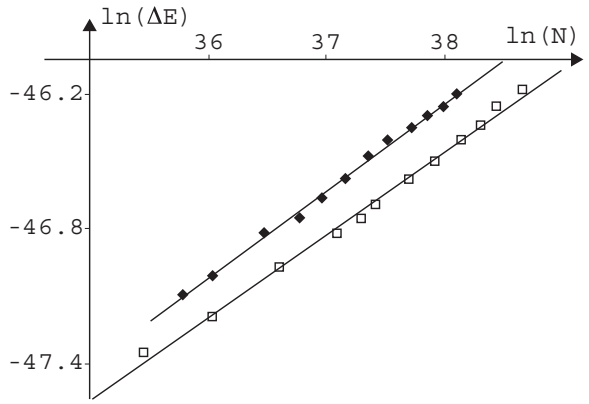

FIG. 2. Experimental data of the band-gap renormalization of an 80 Å (white squares) and a 150 Å (black diamonds) $In_xGa_{1-x}As/InP$ quantum well at 77 K extracted from [46] and replotted to provide the required information. The plot displays $\ln(\Delta E)$ versus $\ln(N)$, where $\Delta\ E = E_t(0) - E_t(N)$ is expressed in joule and N, the surface charge density, in m^{-2} [Eq. (53)]. The continuous lines are the linear best fits. The fitting parameters are $\ln(a) = -60.93 \pm 0.06$ and $b = 0.386 \pm 0.002$ (black diamonds), and $\ln(a) = -60.4 \pm 0.2$ and $b = 0.367 \pm 0.006$ (white squares).

TABLE I. Determination of the Benjamin-Feir stability criterion in the absence ($a = b = 0$) and in the presence of band-gap renormalization for various classes of devices.

Band gap	α	β	$1 + \alpha\beta$
$a = 0$, $b = 0$	−1.00	−0.9068	1.907
Lach *et al.* [45]	3.421	−0.9065	−2.10
Kulakovskii and *et al.* [46], 80 Å	5.118	−0.9060	−3.64
Kulakovskii and *et al.* [46], 150 Å	4.085	−0.9061	−2.71

we select a loss rate (here we use $\sigma = 10^{13}$ Hz), then solve Eq. (6) and determine the critical pump parameter N_{pc} as well as ω_c and k_c through Eq. (8). This allows us to build Table I which provides direct information on the stability. We remark that the Benjamin-Feir stability criterion shows a sudden sign change, from $l_2 < 0$ to $l_2 > 0$, when band-gap renormalization effects are taken into account. Hence, we conclude that, for the classes of devices which we are explicitly considering here, band-gap renormalization induces a phase instability. As band-gap renormalization effects are mainly density carrier corrections, it is mostly the α coefficient which is modified [43], while β remains almost constant, as clearly shown in Table I.

C. Analogy with the complex Ginzburg-Landau equation

Other approximate properties of Eqs. (40) may be inferred from the comparison with the CGLE, for which vast literature exists [47]. In the CGLE the phase instability appears either as pure phase turbulence or as a mixture of phase and amplitude turbulence [27,28]. Although the phase gradients are strongly fluctuating in both cases, in the former the amplitude is almost constant, while in the latter its dynamics is also turbulent. For comparison with the CGLE, even though not entirely justifiable, we perform the standard adiabatic elimination of S (setting $S \simeq \widetilde{\mu} - 4\widetilde{\sigma}|F|^2$ and substituting into the electric field equation), obtaining

$$\partial_T F \simeq c_0\widetilde{\mu}F - V\partial_Z F - 4\widetilde{\sigma}c_0|F|^2F + \epsilon c_1\partial_{ZZ}F + \cdots . \quad (54)$$

By analogy, we then expect (i) a pure phase instability regime for small c_{0i}/c_{0r} and large c_{1i}/c_{1r}, and (ii) an amplitude turbulent regime for large c_{0i}/c_{0r} and small c_{1i}/c_{1r}. In the pure phase instability regime, where the amplitude dynamics is enslaved to that of the phase gradients, the adiabatic elimination of the amplitude leads to the well-known Kuramoto-Sivashinsky phase equation [47] for which the number of positive Lyapunov exponents was shown to linearly increase with the system's size [33]. Thus, we expect the phase instability to act as a "noise generator" for the laser's electric field amplitude.

D. Numerical simulations and comparison with experiments

We have performed numerical simulations of Eqs. (40) using a standard fourth-order Runge-Kutta algorithm for the temporal scheme and a sixth-order finite-difference method to approximate spatial derivatives. We have carefully checked, by using several values of the space and time increments, that the numerical noise does not induce visible effects,

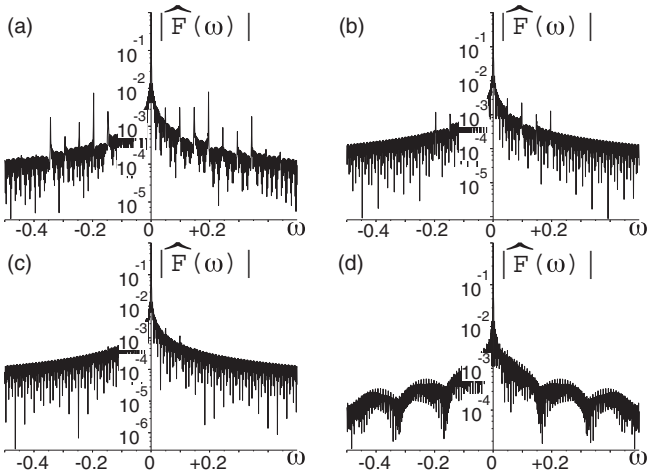

FIG. 3. Log-linear power spectrum of F, from Eqs. (40) at different times, in the phase-stable regime. Some parameters are common to all our simulations: $\widetilde{\mu} = 0.1$, $\widetilde{\sigma} = 2$, $\chi_r = 3$. Specific to this simulation $c_0 = 0.012\,55 + i0.0025$, $c_1 = 1.1955$, $c_2 = 0$. The time increment is 0.05, the space increment 0.125, and the discretization is taken on 1024 points. The spectral components are computed in the time intervals ($\times 10^4$): (a) [1,4], (b) [5,8], (c) [10,13], and (d) [57,60].

at least from a qualitative point of view. Although the experimental results we refer to [14–17] are obtained in the presence of Fabry-Perot-type boundary conditions, here—as is common in numerical work—we use periodic boundary conditions.

Given the long relaxation time scales expected from the phase dynamics, in order to ensure convergence in our simulations we first explore the phase-stable regime. For the parameter values of Fig. 3, the slowest phase gradient decay rate is $\lambda_\phi(\frac{2\pi}{L}) \sim 3 \times 10^{-6}$. Thus, we expect, and *do* observe, that the initial phase gradients vanish after a characteristic time $\tau \sim 10^6$. On the basis of this result, in the following figures we only show predictions obtained in the asymptotic regime. Note that the regular aspect of the power spectrum in the asymptotic regime [Fig. 3(d)] proves numerical noise to be negligible.

By analogy with the CGLE, we associate the numerical observations of Fig. 4 with an amplitude turbulence regime, where not only the phase gradients but also the amplitude strongly fluctuate in space and time. The associated power spectrum is shown in Fig. 5(d). This parameter regime should correspond to the experimental observations obtained far from threshold, where no particular modal sequence was observed and where the total intensity oscillates irregularly [48].

Figure 6 has been numerically obtained in the pure phase-unstable regime (small α, large β). The electric field frequency displays regular variations with asymmetric periodic cycling (the rise time being shorter than the fall time). Only few modes are involved in the dynamics [Fig. 5(c)] and the total intensity is nearly constant. These predictions are in very good qualitative agreement with the experimental observations of deterministic mode switching [14,15], with a sole discrepancy in the intensity bandwidth:

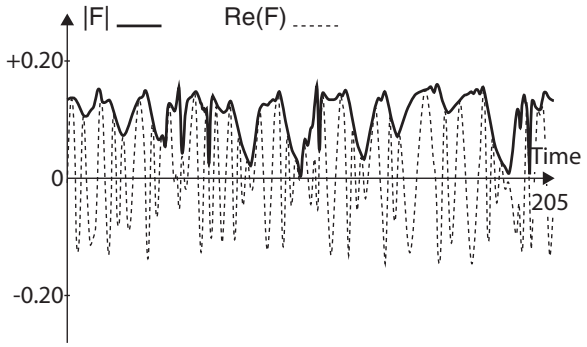

FIG. 4. Numerical simulation of Eq. (40) in the amplitude-turbulent regime. The length L of the numerical box is 512, $c_0 = 0.0050 + i0.0065$, $c_1 = 0.25 - i0.225$, and $c_2 = -i2.5006$. The continuous line stands for the amplitude evolution with time, at a fixed spatial position, and the dashed one for the real part of F versus time. The dynamics is clearly turbulent. The power spectrum is shown in Fig. 5(d).

In the experiment the intermode beatings—if present—could not be detected, while in our calculations they are truly absent.

Finally, we have simulated Eqs. (40) in a phase-stable regime but with the addition of white noise in space and time uniformly distributed between $\pm\zeta\sqrt{dt}$ where dt is the time increment and $\zeta = 4 \times 10^{-3}$. The aim is to compare the effect of externally injected noise to the one intrinsic to the phase instability. Although the latter involves a much narrower frequency range, they both produce multimode dynamics with somewhat differing spectral features [Figs. 5(b) and 5(c)].

IV. CONCLUSION

In conclusion, by computing the normal form description of a semiconductor laser bifurcation near its threshold, we have obtained a general model from which we deduce the existence

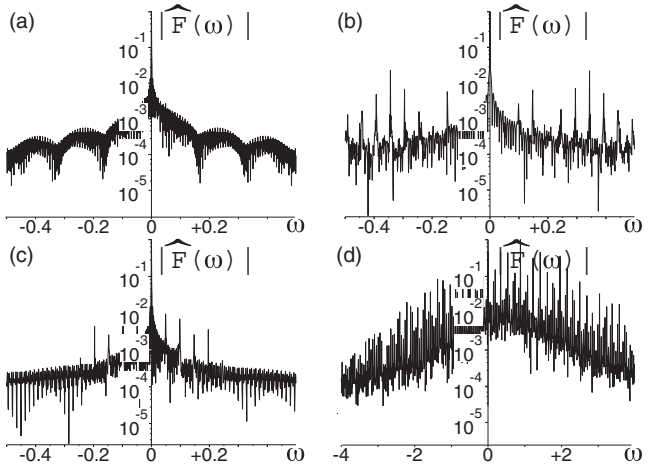

FIG. 5. Typical power spectra of F in a log-linear scale obtained from the integration of Eqs. (40). (a) Phase-stable regime with no added noise corresponding to Fig. 3(d). (b) White noise added on space and time in the regime shown in (a). (c) and (d) Phase-unstable regime (no added noise)—(c) corresponds to the pure phase instability (cf. Fig. 6) and (d) to amplitude turbulence (cf. Fig. 4).

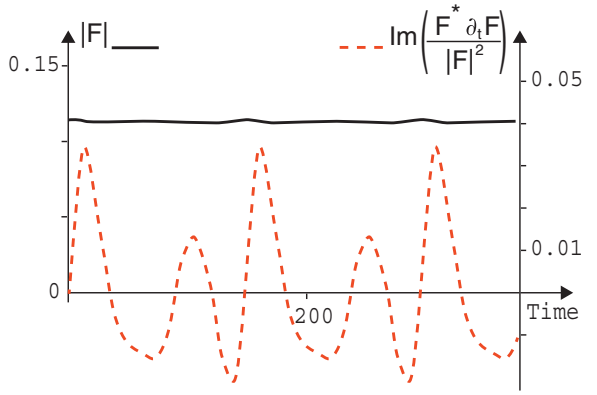

FIG. 6. (Color online) Numerical simulation of Eq. (40) in the pure phase-unstable regime, with $c_0 = 0.0125 + i0.0025$, $c_1 = 1.1955 - i11.9552$, and $c_2 = -i2.5006$. The length L of the numerical box is 119.3984. The solid, top line (black) represents the temporal evolution of the field amplitude, at a fixed spatial position; the dashed, bottom line (red) shows the time derivative of the phase of F [i.e., $\mathrm{Im}(\frac{F^*\partial_t F}{|F|^2})$]. As observed experimentally, the total intensity is constant and the electric field frequency oscillation is not symmetric. The power spectrum is shown in Fig. 5(c).

of a parameter β, proven, both analytically and numerically, to play a crucial role—in conjunction with the well-known α parameter—in the control of the phase instability. Our numerical simulations, predicting (asymmetric) periodic oscillations in the laser frequency, are in good qualitative agreement with the experimental observations [14–17]. Even though material-related noise sources and photon noise sources are always present, and can even be strong in semiconductor devices, our results allow one to consider an interpretation where, in the phase-unstable regime, the external sources of noise may only be an additional accessory which superposes some secondary randomness onto a basically regular (pure phase) or irregular (amplitude turbulence) behavior. Further work is needed to satisfactorily address all the issues related to the simultaneous action of determinism and randomness in these lasers.

APPENDIX A: SERRAT AND MASOLLER'S DESCRIPTION

In [20], the authors derive the following system of equations:

$$\begin{aligned}
\frac{\partial F}{\partial t} &= -\frac{\partial F}{\partial z} + k\left[-i\alpha N + (N-1)\left(1 + G_d\frac{\partial^2}{\partial z^2}\right) - \gamma_{\mathrm{int}}\right]F,\\
\frac{\partial B}{\partial t} &= +\frac{\partial B}{\partial z} + k\left[-i\alpha N + (N-1)\left(1 + G_d\frac{\partial^2}{\partial z^2}\right) - \gamma_{\mathrm{int}}\right]B,\\
\frac{\partial N}{\partial t} &= j - \gamma_n N - (N-1)(|F|^2 + |B|^2) + d\frac{\partial^2 N}{\partial z^2},
\end{aligned} \tag{A1}$$

which possesses a four-continuous-parameter (ϕ_F, ϕ_B, θ, and K) family of solutions

$$\begin{aligned}
F &= R\cos(\theta)e^{i(\Omega t - Kz + \phi_F)},\\
B &= R\sin(\theta)e^{i(\Omega t + Kz + \phi_B)},\\
N &= N_0,
\end{aligned} \tag{A2}$$

with

$$\begin{aligned}
R^2 &= \frac{G_d(\gamma_n - j)K^2 - \gamma_n(\gamma_{\mathrm{int}} + 1) + j}{\gamma_{\mathrm{int}}},\\
N_0 &= \frac{G_d K^2 - \gamma_{\mathrm{int}} - 1}{G_d K^2 - 1},\\
\Omega &= \frac{G_d K^3 - G_d\alpha k K^2 - K + \alpha k(1 + \gamma_{\mathrm{int}})}{G_d K^2 - 1}.
\end{aligned} \tag{A3}$$

Let us look at the linear stability of these solutions, where, for the sake of clarity, we restrict ourselves to the case where $0 = \phi_F = \phi_B = K$ (the case where $K \neq 0$ is not fundamentally different, though).

Among the linear eigenvalues, three are critical. They can expressed as

$$\begin{aligned}
\lambda_1 &= -iq - r_{12}q^2 + \cdots,\\
\lambda_2 &= +iq - r_{12}q^2 + \cdots,\\
\lambda_3 &= i[1 - 2\cos(\theta)^2]q - r_3 q^2 + \cdots,
\end{aligned} \tag{A4}$$

where q is the perturbation wave number and the dots stand for higher powers of q. r_{12} and r_3 are real numbers defined as

$$\begin{aligned}
r_{12} &= k\gamma_{\mathrm{int}}G_d,\\
r_3 &= \frac{2(\gamma_n - j)[\cos(\theta)^2 - \cos(\theta)^4] + G_d\gamma_{\mathrm{int}}^3 k^2(\gamma_{\mathrm{int}}\gamma_n + \gamma_n - j)}{\gamma_{\mathrm{int}}k(\gamma_{\mathrm{int}}\gamma_n + \gamma_n - j)}.
\end{aligned} \tag{A5}$$

For the parameters used in [20], these coefficients turn out to be positive, so that the solutions, Eqs. (A3), are phase stable. In a numerical box of length L, the phase gradients are then expected to decrease with a characteristic time τ given by

$$\tau = \frac{1}{r_{12}\left(\frac{2\pi}{L}\right)^2} \simeq 10^5. \tag{A6}$$

This long characteristic time can lead to confusing a transient with an asymptotic state. This is especially true for the conditions of Ref. [20], where the authors used a time increment $\Delta t = 1/300$ for which the characteristic time τ is reached after $\simeq 10^7$ iterations. Figure 7 displays the long-time evolution of the power spectrum of F in the parameter regime where Ref. [20] identified mode switching. Clearly, the multimode dynamics slowly disappears in favor of a monochromatic one.

APPENDIX B: $\frac{dN}{N_{pc}} = (\frac{\gamma}{\omega_c})^{3/2}$

As discussed in Sec. II C, the scaling choice is not unique. Here we investigate a scaling different from the one discussed previously. Instead of $\frac{dN}{N_{pc}} \propto (\frac{\gamma}{\omega_c})^{1/2}$ we now assume $\frac{dN}{N_{pc}} \propto (\frac{\gamma}{\omega_c})^{3/2}$. We therefore introduce the following scalings:

$$\begin{aligned}
\gamma &= \omega_c\epsilon^2,\\
N_p &= N_{pc}(1 + \widetilde{\mu}\epsilon^3),\\
\sigma &= \omega_c\epsilon\widetilde{\sigma},\\
\Gamma &= \omega_c\epsilon\widetilde{\Gamma},\\
D &= \frac{\omega_c}{k_c^2}\epsilon\widetilde{D},
\end{aligned} \tag{B1}$$

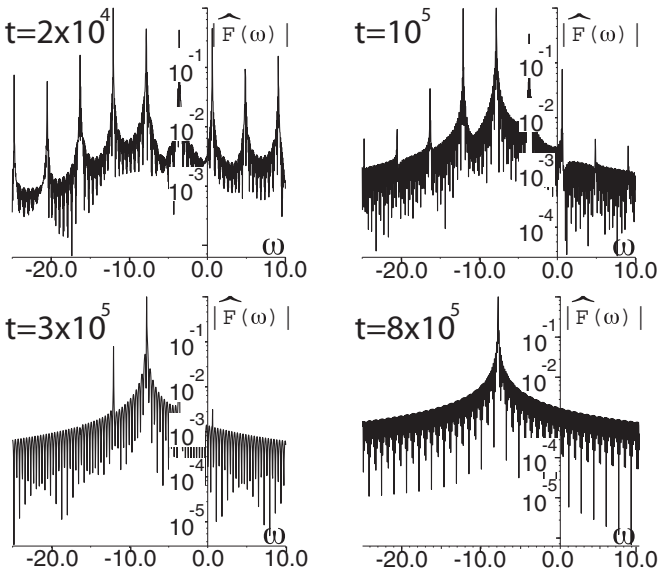

FIG. 7. Numerical simulation of Eq. (A1) with exactly the same parameter values used in [20] for Fig 4(c). The plots show the power spectra of F at different times: 2×10^4, 10^5, 3×10^5, and 8×10^5. The power spectra are computed by integration over a 10^3 time interval in rescaled units. For the first plots, the spectrum is still slowly evolving with time, but it becomes rigorously stationary for the last ones.

with

$$N = N_{pc}(1+\epsilon^3 S+\epsilon^4 N_4+\cdots),$$
$$E = \sqrt{\frac{\omega_c N_{pc}\hbar}{\epsilon_0}}(\epsilon^2 E_2+\epsilon^3 E_3+\cdots),$$
$$\frac{P}{\epsilon_0} = \sqrt{\frac{\omega_c N_{pc}\hbar}{\epsilon_0}}(\epsilon^2 P_2+\epsilon^3 P_3+\cdots), \tag{B2}$$

and

$$\partial_t = \omega_c\left(\partial_{t_0}+\epsilon^4\partial_{t_4}+\epsilon^5\partial_{t_5}+\cdots\right),$$
$$\partial_z = k_c\left(\partial_{z_0}+\epsilon^3\partial_{z_3}+\cdots\right). \tag{B3}$$

At order ϵ^2 solvability requires

$$\partial_{t_0t_0}(E_2+P_2) = \frac{c^2k_c^2}{\omega_c^2}\partial_{z_0z_0}E_2 \tag{B4}$$

and a possible solution is

$$E_2 = Fe^{i(t_0-z_0)}+\text{c.c.},$$
$$P_2 = \chi_r Fe^{i(t_0-z_0)}+\text{c.c.} \tag{B5}$$

At order ϵ^3,

$$\partial_{t_0t_0}(E_3+P_3) = -\widetilde{\sigma}\partial_{t_0}E_2+\frac{c^2k_c^2}{\omega_c^2}\partial_{z_0z_0}E_3,$$
$$\partial_{t_0}S = 0. \tag{B6}$$

A possible solution is then

$$E_3 = 0,$$
$$P_3 = i\widetilde{\sigma}Fe^{i(t_0-z_0)}+\text{c.c.},$$
$$\partial_{t_0}S = 0. \tag{B7}$$

At order ϵ^4,

$$\partial_{t_0t_0}(E_4+P_4) = \frac{c^2k_c^2}{\omega_c^2}\partial_{z_0z_0}E_4,$$
$$\partial_{t_0}N_4 = \widetilde{D}\partial_{z_0z_0}S+2E_2\partial_{t_0}P_2. \tag{B8}$$

A possible solution is

$$E_4 = 0,$$
$$P_4 = 0,$$
$$N_4 = \chi_r F^2e^{2i(t_0-z_0)}+\text{c.c.},$$
$$\partial_{z_0}S = 0. \tag{B9}$$

At order ϵ^5,

$$\partial_{t_0t_0}(E_5+P_5) = \frac{c^2k_c^2}{\omega_c^2}\left(\partial_{z_0z_0}E_5+2\partial_{z_0z_3}E_2\right),$$
$$\partial_{t_0}N_5 = \widetilde{\mu}-S+\widetilde{D}\partial_{z_0z_0}N_4+2E_2\partial_{t_0}P_3. \tag{B10}$$

Looking for a solution of the form

$$E_5 = F_5e^{i(t_0-z_0)}+\text{c.c.} \tag{B11}$$

leads to

$$P_5 = e^{i(t_0-z_0)}\left[\chi_r F_5+N_{pc}\frac{\partial\chi}{\partial N}SF_2-i\chi_\omega\partial_{t_4}F_2\right]+\text{c.c.} \tag{B12}$$

Collecting terms, the solvability conditions are expressed as

$$\partial_{t_4}F = -V\partial_{z_3}F+c_0SF,$$
$$0 = \widetilde{\mu}-S-4\widetilde{\sigma}|F|^2, \tag{B13}$$

which shows that there is no dynamics associated with S. We can interpret this result in the following way: With this particular scaling choice, the dynamics of the electric field amplitude is so slow, compared to $\frac{\gamma}{\omega_c}$, that the carrier density plays the role of a fast variable; thus it can be adiabatically eliminated.

APPENDIX C: $\frac{dN}{N_{pc}} = (\frac{\gamma}{\omega_c})^{1/3}$

The last scaling choice announced in Sec. II C requires the following scalings:

$$\gamma = \omega_c\epsilon^6,$$
$$N_p = N_{pc}(1+\widetilde{\mu}\epsilon^2),$$
$$\sigma = \omega_c\epsilon^3\widetilde{\sigma},$$
$$\Gamma = \omega_c\epsilon^3\widetilde{\Gamma},$$
$$D = \frac{\omega_c}{k_c^2}\epsilon^3\widetilde{D}, \tag{C1}$$

with

$$N = N_{pc}(1+\epsilon^2 S+\epsilon^3 N_3+\epsilon^4 N_4+\cdots),$$
$$E = \sqrt{\frac{\omega_c N_{pc}\hbar}{\epsilon_0}}(\epsilon^{5/2}E_{5/2}+\epsilon^{7/2}E_{7/2}+\cdots),$$
$$\frac{P}{\epsilon_0} = \sqrt{\frac{\omega_c N_{pc}\hbar}{\epsilon_0}}(\epsilon^{5/2}P_{5/2}+\epsilon^{7/2}P_{7/2}+\cdots), \tag{C2}$$

and

$$\partial_t = \omega_c(\partial_{t_0} + \epsilon^5\partial_{t_5} + \epsilon^6\partial_{t_6} + \cdots),$$
$$\partial_z = k_c(\partial_{z_0} + \epsilon^2\partial_{z_2} + \epsilon^3\partial_{z_3} + \cdots). \quad \text{(C3)}$$

Note that, although we used the same ϵ for the previous two choices of exponents ($r = \frac{3}{2}$ and $r = \frac{1}{2}$), here we have redefined it, Eq. (C1), in order to minimize the manipulation of fractional exponents.

At order ϵ^2 solvability requires

$$\partial_{t_0} S = 0. \quad \text{(C4)}$$

At order $\epsilon^{5/2}$,

$$\partial_{t_0 t_0}(E_{5/2} + P_{5/2}) = \frac{c^2k_c^2}{\omega_c^2}\partial_{z_0 z_0} E_{5/2}. \quad \text{(C5)}$$

A solution is now

$$E_{5/2} = Fe^{i(t_0 - z_0)} + \text{c.c.}, \quad P_{5/2} = \chi_r E_{5/2}. \quad \text{(C6)}$$

At order ϵ^3,

$$\partial_{t_0} N_3 = \widetilde{D}\partial_{z_0 z_0} S, \quad \text{(C7)}$$

with solution

$$N_3 = 0, \quad \partial_{z_0} S = 0. \quad \text{(C8)}$$

At order $\epsilon^{7/2}$,

$$\partial_{t_0 t_0}(E_{7/2} + P_{7/2}) = \frac{c^2k_c^2}{\omega_c^2}\partial_{z_0 z_0} E_{7/2}, \quad \text{(C9)}$$

whose solution is

$$E_{\frac{7}{2}} = 0 = P_{7/2}. \quad \text{(C10)}$$

At order ϵ^4,

$$\partial_{t_0} N_4 = 0, \quad \text{(C11)}$$

whose trivial solution is

$$N_4 = 0. \quad \text{(C12)}$$

At order $\epsilon^{9/2}$,

$$\partial_{t_0 t_0}(E_{9/2} + P_{9/2}) = \frac{c^2k_c^2}{\omega_c^2}\left(\partial_{z_0 z_0} E_{9/2} + 2\partial_{z_0 z_2} E_{5/2}\right). \quad \text{(C13)}$$

Looking for a solution for $E_{9/2}$ of the form $(F_{9/2}e^{i(t_0 - z_0)} + \text{c.c.})$ leads to

$$P_{9/2} = e^{i(t_0 - z_0)}\left[\chi_r F_{9/2} + N_{pc}\frac{\partial\chi}{\partial N} S F_{5/2} - i\chi_\omega \partial_{t_5} F_{5/2}\right] + \text{c.c.} \quad \text{(C14)}$$

The solvability condition is expressed as

$$\partial_{t_5} F_{5/2} = -V\partial_{z_2} F_{5/2} + c_0 S F_{5/2}, \quad \text{(C15)}$$

where c_0 and V are the same as those previously defined in the main text, Eq. (32). Then a possible solution is

$$E_{9/2} = 0, \quad P_{9/2} = \frac{2ic^2k_c^2}{\omega_c^2}\partial_{z_2} F_{5/2} e^{i(t_0 - z_0)} + \text{c.c.} \quad \text{(C16)}$$

At order ϵ^5,

$$\partial_{t_0} N_5 = 2E_{5/2}\partial_{t_0} P_{5/2}, \quad \text{(C17)}$$

whose solution is

$$N_5 = \chi_r F_{5/2}^2 e^{2i(t_0 - z_0)} + \text{c.c.} \quad \text{(C18)}$$

At order $\epsilon^{11/2}$,

$$\partial_{t_0 t_0}(E_{11/2} + P_{11/2}) = -\widetilde{\sigma}\partial_{t_0} F_{5/2} + \frac{c^2k_c^2}{\omega_c^2}\left(\partial_{z_0 z_0} E_{11/2} + 2\partial_{z_0 z_3} E_{5/2}\right). \quad \text{(C19)}$$

Looking for a solution for $E_{11/2}$ of the form $(F_{11/2}e^{i(t_0 - z_0)} + \text{c.c.})$ we obtain

$$P_{11/2} = \left[\chi_r F_{11/2} + i\widetilde{\sigma} F_{5/2} - i\chi_\omega \partial_{t_6} F_{5/2}\right]e^{i(t_0 - z_0)} + \text{c.c.} \quad \text{(C20)}$$

The solvability condition is

$$\partial_{t_6} F_{5/2} = -V\partial_{z_3} F_{5/2}, \quad \text{(C21)}$$

which just corresponds to a renormalization of Eq. (C15). When this condition is satisfied, a possible solution is

$$E_{11/2} = 0,$$
$$P_{11/2} = \left[i\widetilde{\sigma} F_{5/2} + \frac{2ic^2k_c^2}{\omega_c^2}\partial_{z_3} F_{5/2}\right]e^{i(t_0 - z_0)}. \quad \text{(C22)}$$

At order ϵ^6,

$$\partial_{t_0} N_6 = \widetilde{D}\partial_{z_0 z_0} N_5, \quad \text{(C23)}$$

which leads to

$$N_6 = 2i\chi_r \widetilde{D} F_{5/2}^2 e^{2i(t_0 - z_0)} + \text{c.c.} \quad \text{(C24)}$$

At order $\epsilon^{13/2}$,

$$\partial_{t_0 t_0}(E_{13/2} + P_{13/2}) = \frac{c^2k_c^2}{\omega_c^2}\left[\partial_{z_0 z_0} E_{13/2} + \left(2\partial_{z_0 z_4} + \partial_{z_2 z_2}\right)E_{5/2}\right]. \quad \text{(C25)}$$

Looking for a solution of the form

$$E_{13/2} = F_{13/2}e^{i(t_0 - z_0)} + G_{13/2}e^{3i(t_0 - z_0)} + \text{c.c.}, \quad \text{(C26)}$$

we find

$$P_{13/2} = e^{i(t_0 - z_0)}\begin{bmatrix}\chi_r F_{13/2} \\ +\frac{1}{2}\frac{\partial^2\chi}{\partial N^2} N_{pc}^2 S^2 F_{5/2} - i\chi_\omega \partial_{t_7} F_{5/2} \\ -i\chi_\omega N_{pc} S\partial_{t_5} F_{5/2} - \frac{\chi_{\omega\omega}}{2}\partial_{t_5 t_5} F_{5/2}\end{bmatrix} + e^{3i(t_0 - z_0)}[\cdots] + \text{c.c.} \quad \text{(C27)}$$

The solvability condition now takes the form

$$i\chi_\omega \partial_{t_7} F_{5/2} = -\frac{1}{2}\frac{\partial^2\chi}{\partial N^2} N_{pc}^2 S^2 F_{5/2} + i\chi_\omega N_{pc} S\partial_{t_5} F_{5/2} + \frac{\chi_{\omega\omega}}{2}\partial_{t_5 t_5} F_{5/2} + \frac{c^2k_c^2}{\omega_c^2}\left(-2i\partial_{z_4} + \partial_{z_2 z_2}\right)F_{5/2}. \quad \text{(C28)}$$

Comparing the previous equation with Eq. (39), we find that they are nearly identical, save for the term $\frac{\partial\chi}{\partial N} N_{pc}[N_2 E_1]_1$ which is present in Eq. (39) but not here. An equivalent to this term will appear at order $\epsilon^{15/2}$ as $[N_5 E_{5/2}]_1$.

At order ϵ^7,

$$\partial_{t_0} N_7 + \partial_{t_5} S = \widetilde{D}\left(\partial_{z_0 z_0} N_6 + \partial_{z_2 z_2} S\right) + 2E_{\frac{5}{2}}\partial_{t_0} P_{9/2}, \quad \text{(C29)}$$

and the solvability condition is expressed as

$$\partial_{t_5} S = \widetilde{D}\partial_{z_2 z_2} S - \frac{4c^2 k_c^2}{\omega_c^2}\partial_{z_2}|F_{5/2}|^2. \tag{C30}$$

Comparing with Eq. (32), we find that some terms are missing (e.g., $(\widetilde{\mu} - S)$, which will appear at order ϵ^8], while new ones are emerging (e.g., $\partial_{z_2 z_2} S$).

In conclusion, whatever the initial scaling choice [$\frac{dN}{N_{pc}} \propto (\frac{\gamma}{\omega_c})^{1/2}$ or $\propto(\frac{\gamma}{\omega_c})^{1/3}$], and for an infinite expansion order, the two final normal form descriptions are identical. However, for a finite expansion order, the two approaches may differ and the choice of the remaining terms is then based on their physical relevance and the physical phenomena to be modeled.

[1] J. R. Tredicce, F. T. Arecchi, G. L. Lippi, and G. P. Puccioni, J. Opt. Soc. Am. B **2**, 173 (1985).
[2] F. T. Arecchi and R. Bonifacio, IEEE J. Quantum Electron. **QE-1**, 169 (1965).
[3] L. M. Narducci and N. B. Abraham, *Laser Physics and Laser Instabilities* (World Scientific, Singapore, 1988).
[4] R. Linke, B. Kasper, C. Burrus, I. Kaminow, J. Ko, and T. P. Lee, J. Lightwave Technol. **3**, 706 (1985).
[5] M. Ohtsu and Y. Teramachi, IEEE J. Quantum Electron. **25**, 31 (1989).
[6] M. Ohtsu, Y. Teramachi, Y. Otsuka, and A. Osaki, IEEE J. Quantum Electron. **22**, 535 (1986).
[7] R. W. Tkach and A. R. Chraplyvy, IEEE J. Lightwave Technol. **4**, 1655 (1986).
[8] I. Wallace, Dejin Yu, R. G. Harrison, and A. Gavrielides, J. Opt. B.: Quantum Semiclassical Opt. **2**, 447 (2000).
[9] G. Huyet, S. Balle, M. Giudici, C. Green, G. Giacomelli, and J. R. Tredicce, Opt. Commun. **149**, 341 (1998).
[10] G. R. Gray and R. Roy, J. Opt. Soc. Am. B **8**, 632 (1991).
[11] D. Lenstra, B. H. Verbeek, and A. J. den Boef, IEEE J. Quantum Electron. **21**, 674 (1985).
[12] G. Vaschenko, M. Giudici, J. J. Rocca, C. S. Menoni, J. R. Tredicce, and S. Balle, Phys. Rev. Lett. **81**, 5536 (1998).
[13] G. Huyet, J. K. White, A. J. Kent, S. P. Hegarty, J. V. Moloney, and J. G. McInerney, Phys. Rev. A **60**, 1534 (1999).
[14] A. M. Yacomotti, L. Furfaro, X. Hachair, F. Pedaci, M. Giudici, J. R. Tredicce, J. Javaloyes, S. Balle, E. A. Viktorov, and P. Mandel, Phys. Rev. A **69**, 053816 (2004).
[15] L. Furfaro, F. Pedaci, M. Giudici, X. Hachair, J. R. Tredicce, and S. Balle, J. Quantum Electron. **40**, 1365 (2004).
[16] M. Yamada, M. Ishimori, H. Sakaguchi, and M. Ahmed, J. Quantum Electron. **39**, 1548 (2003).
[17] Y. Tanguy, J. Houlihan, G. Huyet, E. A. Viktorov, and P. Mandel, Phys. Rev. Lett. **96**, 053902 (2006).
[18] M. Ahmed, Physica D **176**, 212 (2003).
[19] S. Balle, Phys. Rev. A **57**, 1304 (1998).
[20] C. Serrat and C. Masoller, Phys. Rev. A **73**, 043812 (2006).
[21] L. Gil and G. L. Lippi, Proc. SPIE **9134**, 913413 (2014).
[22] L. Gil and G. L. Lippi, Phys. Rev. A **83**, 043840 (2011).
[23] G. Iooss and M. Adelmeyer, *Topics in Bifurcation Theory and Applications* (World Scientific, Singapore, 1998).
[24] M. Clerc, P. Coullet, and E. Tirapegui, Phys. Rev. Lett. **83**, 3820 (1999).
[25] L. Gil and G. L. Lippi, Phys. Rev. Lett. (to be published).
[26] T. B. Benjamin and J. E. Feir, J. Fluid Mech. **27**, 417 (1967).
[27] B. I. Shraiman, A. Pumir, W. van Saarloos, P. C. Hohenberg, H. Chaté, and M. Holen, Physica D **57**, 241 (1992).
[28] H. Chaté, Nonlinearity **7**, 185 (1994).
[29] J. A. Copeland, J. Appl. Phys. **54**, 2813 (1983).
[30] C. H. Henry, P. S. Henry, and M. Lax, J. Lightwave Technol. **2**, 209 (1984).
[31] R. H. Wentworth, IEEE J. Quantum Electron. **26**, 426 (1990).
[32] M. Ahmed and M. Yamada, IEEE J. Quantum Electron. **38**, 682 (2002).
[33] P. Manneville, in *Macroscopic Modelling of Turbulent Flows*, edited by U. Frisch, J. Keller, G. Papanicolau, and O. Pironneau, Lecture Notes in Physics Vol. 230 (Springer, Berlin, 1985), pp. 319–326.
[34] M. Osinski and J. Buus, IEEE J. Quantum Electron. **23**, 9 (1987).
[35] C. H. Henry, J. Lightwave Technol. **4**, 288 (1986).
[36] Normal form computations are rigorously derived near a bifurcation threshold. However, because they fully capture the symmetries of the problem, their actual validity domain usually turns out to be much larger.
[37] W. W. Chow and S. W. Koch, *Semiconductor-Laser Fundamentals* (Springer, Berlin, 1999).
[38] C. Harder, K. Vahala, and A. Yariv, Appl. Phys. Lett. **42**, 328 (1983).
[39] C. Z. Ning, R. A. Indik, and J. V. Moloney, IEEE J. Quantum Electron. **33**, 1543 (1997).
[40] J. Javaloyes and S. Balle, Phys. Rev. A **81**, 062505 (2010).
[41] Exercise 2-11 in A. C. Newell and J. V. Moloney, *Nonlinear Optics* (Addison-Wesley, Redwood, CA, 1992).
[42] G. L. Oppo and A. Politi, Europhys. Lett. **1**, 549 (1986).
[43] The usual α factor is defined as the ratio between the derivatives of the real and imaginary parts of the susceptibility with respect to the carrier density N *at transparency*. Our α coefficient is defined *at threshold*, i.e., for the smallest value of the pump N_{pc} for which the vanishing solution becomes unstable. Hence defined, our α coefficient depends explicitly on the losses through N_{pc}, which is clearly more satisfactory from a theoretical and an experimental point of view.
[44] Our susceptibility expression slightly differs from [19] because the electric field is expressed as $E = Fe^{i(kz-\omega t)} + \text{c.c.}$ in [19], while we use the opposite convention $E = Fe^{i(\omega t - kz)} + \text{c.c.}$.
[45] E. Lach, A. Forchel, D. A. Broido, T. L. Reinecke, G. Weimann, and W. Schlapp, Phys. Rev. B **42**, 5395(R) (1990).
[46] V. D. Kulakovskii, E. Lach, A. Forchel, and D. Grützmacher, Phys. Rev. B **40**, 8087(R) (1989).
[47] I. S. Aranson and L. Kramer, Rev. Mod. Phys. **74**, 99 (2002).
[48] X. Hachair (private communication).